LAWRENCE
LIVERMORE
NATIONAL
LABORATORY

LLNL-TR-432813

Numerical modeling to assess the sensitivity and resolution of long-electrode electrical resistance tomography (LEERT) surveys to monitor CO2 migration, Phase 1B area

A. L. Ramirez

May 20, 2010

Disclaimer

This work performed under the auspices of the U.S. Department of Energy by Lawrence Livermore National Laboratory under Contract DE-AC52-07NA27344.

Theme 3B: Storage Monitoring Methods
Task 3A.6 Numerical Modeling Electrical Resistance Tomography

Numerical modeling to assess the sensitivity and resolution of long-electrode electrical resistance tomography (LEERT) surveys to monitor CO_2 migration, Phase 1B area

Abelardo L. Ramirez
Lawrence Livermore National Laboratory

LLNL-TR-432813

Introduction

If geologic formations are to be used to sequester CO_2 for long time periods, it will be necessary to monitor the reservoir containing the CO_2. Monitoring is necessary to confirm the containment of CO_2, assess leakage paths, and gain understanding into interactions between CO_2, the formation and formation fluids. Remote methods are preferred, both to minimize disruption and to reduce costs. Time-lapse seismic reflection measurements have been successfully used to monitor CO_2 distributions in the Weyburn-Midale reservoir. However, The spatial distribution of CO_2 saturations cannot be determined uniquely through seismic reflection surveys alone. This document explores the possibility of using electrical methods to supplement the seismic reflection surveys.

Electrical methods are well suited for monitoring processes involving fluids. The electrical properties of geologic systems depend on many of the same factors relevant to CO_2 sequestration. The electrical resistivity and impedance of rocks and soils depend on: water saturation, the amount and type of ions in the water, pH, cation exchange capacity of the minerals, and on temperature. As a result of these dependencies, high resolution tomograms of electrical properties have been used with success for both site characterization and to monitor subsurface migration of various fluids such as subsurface steam floods, underground tank leaks, water infiltration events, and contaminant movement (Binley et al., 1996, Binley et al., 2001, Daily et al., 1992; Daily et al., 2000; Kemna, et al. 2000, LaBrecque et al., 1996, LaBrecque and Yang 2000, Loke and Barker, 1995, Oldenburg and Li, 1994, Ramirez *et al.*, 1993, Ramirez *et al.*, 1995, Ramirez *et al.*, 1996, Sasaki, 1994, Schima et al., 1996, Slater et al., 1997a, 1997b). Electrical imaging techniques have also been used successfully to monitor the integrity of subsurface barriers (Daily and Ramirez, 2000), and monitor changes in saturation caused

by heater tests in welded tuff (Ramirez and Daily, 2001). High-resolution field surveys such as these are typically conducted using subsurface "point" electrode arrays in a cross-well configuration. By "point" electrode we mean that the electrode size is much smaller than the distance separating adjacent electrodes.

Metal-cased boreholes are common in typical oil reservoirs and are electrically conductive. The casings can be used as long electrodes, thus permitting the same infrastructure to have both an operational and a monitoring role (refer to Figure 1). A relatively uncommon strategy in the electrical resistivity imaging method is the use of existing subsurface infrastructure to image the reservoir. Ramirez et al., 1996 and Shi et al., 1997 report on environmental and geothermal studies where steel casings were used as long electrodes in combination with point electrodes to produce useful three-dimensional ERT tomograms. Specialized hardware that can produce, measure and switch currents of 10 amperes or higher (at about 100V) is required to use steel casings as long electrodes. If such imaging can be performed using operational casings as electrodes, this provides a nearly noninvasive method for monitoring the CO_2 injection process, and for verifying the spatial distribution of CO_2 within the reservoir. We call this approach long-electrode ERT (LEERT).

The objective is to produce time dependent maps of changes in formation resistivity caused by CO_2 injection and migration. Using the existing subsurface infrastructure would require no additional drilling. Vertical wells alone can provide some information regarding the lateral changes in a field. If metal-cased horizontal wells are available, some vertical resolution may be provided as well. ERT surveys can be made in an automated, remote fashion; these capabilities translate into lower costs. The ability to conduct surveys at any time, without disrupting operations, is highly desirable. This is in contrast with conventional cross-well and logging surveys, which often require the removal of pumps and tubing from wells, thereby disrupting injection or production operations. In addition to providing insight into injection/sequestration performance over time, such surveys would provide a context for decisions regarding the deployment of more focused (and more expensive) survey methods such as the high-resolution 3D seismic technique.

This document describes the results of a numerical modeling study that evaluated whether LEERT could be used successfully to monitor CO_2 distribution in the Weyburn-Midale reservoir, Phase 1B area. The magnitude of electrical resistivity changes and the technique's resolution depend on many site-specific factors including well separation distances, casing lengths, reservoir depth, thickness, and composition, and the effect of CO_2 on the electrical properties of the reservoir. Phase 1B-specific numerical modeling of the electrical response to CO_2 injection has been performed to assess sensitivity and resolution of the electrical surveys.

Approach description

Study Scope

The sensitivity and resolution of LEERT are dependent on a number of factors. These include: 1) the electrical resistivity contrast between an anomaly and the background, 2) the anomaly location (particularly its proximity to the electrodes), 3) the length of the casings, 4) anomaly size and shape, 5) the presence of other metal conductors (i.e., metal-cased wells not used as electrodes), 6) signal-to-noise ratios and measurement error, and 7) the objective function used to stabilize the inversion algorithm. Our study was designed to explore items 2, 3, 4, 5 and 6.

Using Phase 1B - specific information we developed a set of models representing realistic CO_2 injection scenarios. Numerical simulations were conducted to investigate realistic LEERT deployment scenarios that could be implemented using abandoned wells and water after gas (WAG wells). We consider two distinct well configurations: 1) Eight abandoned wells near the Phase 1B area were used to "collect the data". 2) An additional 22 WAG wells were also used to conduct the surveys. We also consider a case were the casing length and reservoir depth is only 820 m (shallowest depth at which CO_2 will remain supercritical) to assess the effect of the length of the casings on the results. For each well configuration, the modeling predicted the electrical response at two times: (a) after 1.4 years of CO_2 injection, and (b) after 5.7 years of CO_2 injection.

The usefulness of metal casings as electrodes depends on whether the injected current pathway is only through the ground. Surface metal pipes and the water volume within them connecting the borehole may be important current pathways, thereby reducing or eliminating the usefulness of the casings as long electrodes. We believe that there are reasonable modifications that can be made to the surface pipes to prevent significant current flow trough them. Discussion of these modifications is outside of the scope of this study. Here we assume that the effect of surface piping on current flow is negligible.

Figure 2 shows a Map view of the Phase 1B area and the location of wells containing metallic casings. Yellow triangles represent the 8 abandoned wells, blue diamonds represent the WAG wells, and green squares represent the oil producers. The red circles represent the vertical, metal cased segment of the CO_2 injection wells active at the beginning of Phase 1B injection. The dashed red line approximately indicates injectors' segments that are horizontal and uncased.

Figure 3 schematically illustrates how current flows when long electrodes are used. A challenging characteristic of the LEERT method is that the long electrodes inject almost all the current in the rock above the reservoir. This means that typically there is very low current flowing in the reservoir and therefore low sensitivity to reservoir changes. In the Phase 1B area, this is especially true because the metallic casings terminate near the top of the reservoir; only a tiny fraction of the current reaches the reservoir. In addition, the casings act as very conductive pathways that substantially distort the electric field in the reservoir. This study evaluates both of these effects.

We considered modifications to the abandoned wells that could increase the amount of current interrogating the reservoir layer and could be implemented cost-effectively. Figure 4 shows three electrode deployment scenarios considered in this study. One scenario includes casings terminating at 1420 m depth (near the top of the reservoir, left part of the figure); this scenario is called deployment 1. We also consider a scenario where the reservoir's top and the casings' ends are located at 820 m to test the influence of casing length on sensitivity); this scenario is called "deployment 1 shallow".

Two other electrode scenarios (shown in the middle and right parts of Figure 4) evaluate whether simple modifications to the abandoned wells would produce better electrical contact with the reservoir. One scenario assumes that a steel wire rope reaches below the end of abandoned casing into the reservoir layer; this scenario is called "deployment 2". The next scenario assumes short electrodes lowered to reservoir depths and connected to the surface via insulated cables; this scenario is called deployment 3.

Site-specific model

We consider two injection volume scenarios for this study (refer to Figure 5). One case assumes injection over a 1.4 year period and another case assumes injection over a 5.7 year period. We assume that the CO_2 causes a fourfold increase in resistivity based on the work of Albright (1984). He showed time-lapse electrical logs collected in dolomitic sands during CO_2 injection that indicated that the resistivity increased by a factor of about 4. We also assume that the reservoir layer is more resistive than layers above and below; this assumption is based on electrical logs from the Weyburn site.

We made the following assumptions to determine the size of the anomalies in Figure 5. 1) The CO_2 injection rate averages about 2600 SCM per month per well; this average was computed using injection data from Phase 1B wells. 2) There are two horizontal injection wells that are approximately collinear as shown in Figure 2. 3) The average reservoir porosity is assumed to be 0.10 and the average CO_2 saturation within the plume is 0.5. We used these numbers to estimate the rock volume that would contain the plume after 1.4 and 5.7 years of injection; the anomalies in Figure 5 represent these rock volumes.

We used a 3D, finite difference algorithm described by LaBrecque, et al. (1999) to solve the forward and inverse problems. Three-dimensional resistivity inversion by nature is ill-posed and underdetermined. Inverse solutions that consider only matching the predicted data to the observations are non-unique and do not behave robustly. The algorithm used here is based on an Occam's type inversion that yields a minimum roughness solution that is consistent with the data and their errors. The algorithm uses a regularized solution (Tikhonov and Arsinen 1977) to improve robustness and reduce non-uniqueness. It jointly minimizes the data misfit between the predicted and observed data and the solution roughness, thereby stabilizing the inverted value of the parameters.

Predicted signal-to-noise and current density

We compare the predicted signal-to-noise ratios (SNR) associated with scenarios described earlier to those that have been observed in previous field projects to assess whether or not the Phase 1B injection signals are likely to provide reliable reservoir information. We compare the magnitude of the predicted resistance measurements and the changes caused by the plume to our previous experiences in the field with this technology.

Figures 6 and 7 show the predicted SNR for some of the deployment scenarios considered. The plots show the magnitude of the resistances (plotted along the abscissa, resistance = received voltage/transmitted current) that would be measured given the "before injection" resistivity model. Each circle represents a resistance measured using different combinations of electrodes. A resistance of 10^{-5} ohms indicates that the voltage measured at the receiver will be 10^{-4} volts if the transmitted current is 10 amperes. The predicted percent change in resistance caused by 1.4 and 5.7 years of CO_2 injection is plotted along the ordinate. We believe that both the magnitude and the percent change in resistance have to be above some threshold in order for the measurement to provide useful information for monitoring CO_2 plumes. Based on previous field deployments, we believe that resistance measurements with magnitudes > 10^{-5} ohms and percent changes larger than 2% (points above and to the right of the red arrows in Figures 6 and 7) are likely to have acceptable signal to noise ratios (SNR), and therefore, be useful for tomography inversions.

Figures 6 shows the SNR for deployments 1 and 1-shallow. This scenario assumes that only the 8 abandoned well casings are used as long electrodes. The plots indicate that none of the measurements are above the thresholds indicated by the red arrows. We conclude that none of the measurements are likely to have acceptable SNR. We need to explore reasonable modifications to this scenario in order to have a chance at detecting the CO_2 anomaly.

Figure 7 shows the same type of plots for the case where the 8 abandoned casings are supplemented by 22 well casings. The change in resistivity caused by 1.4 and 5.7 years of CO_2 injection (dark blue triangles and light blue circles, respectively) is shown. Note that the additional long electrodes produce some data that are likely to show acceptable SNR. Some of the extra electrodes reduce the electrode-CO_2 anomaly distance thereby improving the SNR for some of the measurements. The left graph (associated with deployment 1) shows that 1.1 % and 4.7 % of the measurements (1.4 and 5.7 years after injection, respectively) are predicted to have acceptable SNR. The right graph (associated with deployment 1 - shallow) shows that 1.1 % and 7.1 % of the measurements are predicted to have acceptable SNR. We did a similar analysis for deployments 2 and 3 data (deployment 2: 1.1 % and 4.9%, deployment 3: 0% and 0%).

These results suggest that none of the deployment scenarios considered are likely to produce enough data with adequate SNR and sensitivity to allow successful inversion of ERT data. Specifically, a small fraction of the measurements produced by deployments 1 and 2 will be able to detect the CO_2 anomalies while deployment 3 does not offer any

detection capability. It appears that the number of "good" measurements is insufficient to resolve the shape and location of the plume. We believe, based on past experience, that good resolution can be achieved when at least 30 % of the measurements have sufficient sensitivity to the plume and have good SNR.

We can use other analyses to evaluate whether useful data can be collected. Current density can be used as an indicator of sensitivity because it is directly proportional to electric field strength (volts/m). As a result, a CO_2 anomaly in a high-density region produces larger voltage changes that are more likely to be detected. It helps to understand how sensitivity varies spatially within the region of interest. Current density also helps explain the impact that resistive anomalies (like CO_2) and conductive anomalies (like other casings that are not used as electrodes) have on current flow. We will use current density maps to further evaluate the 22 electrode scenarios.

Figure 8 shows horizontal slices through 3D current density maps. The left image illustrates the scenario where that the top of the reservoir and the bottom of the casings are located at 1420 m (deployment 1 scenario). The right image illustrates the scenario where that the top of the reservoir and the bottom of the casings are located at 820 m (deployment 1-shallow). The slice is located in the reservoir layer, about 20 m below the bottom of the casings. The current injected by each electrode is 1 Ampere. The maps show that the highest current densities exist directly below the casing ends. This means that electrodes located closest to the CO_2 plume will provide the largest sensitivity. A comparison of the two Figure 8 images indicates that higher current densities are shown in the right image, especially in the regions between electrodes. Given the same amount of current, shorter casing lengths produce higher densities and consequently, higher sensitivities.

Also notice the dark colored rectangles located near the top of both Figure 8 images. These indicate regions of relatively low current density caused by the presence of the high-resistivity CO_2 anomalies. The images suggest that most of the current flows around the anomalies rather than though it. This makes it more difficult to estimate the CO_2 saturation within the plumes. Ramirez et al. (2003) discuss in more detail the implications of having less sensitivity to the interior of the CO_2 plume. In addition, we know that the reservoir layer has a higher resistivity than the layer above (see side view of the resistivity model in Figure 5). This condition also causes more of the current to flow around instead of through the reservoir layer, thereby further reducing sensitivity to the CO_2 plume.

Deployment scenarios 2 and 3 were conceived as possible abandoned well modifications that might increase sensitivity to CO_2 within the reservoir layer. The left image in Figure 9 shows the current density predicted for deployment 2: a steel wire rope has been inserted into each abandoned well to increase the electrical coupling and amount of current reaching the reservoir layer. This image can be compared to the left image in Figure 8 because both consider the same scenario (excepting the addition of the wire rope).

The comparison suggests that the changes in current density caused by the adding the wire rope are small or negligible. This suggests that electrical coupling with the reservoir is not likely to be the primary condition affecting measurement sensitivity. We believe that the large inter-electrode distance is likely to be the dominant condition responsible for low measurement sensitivity. Previous work (Ramirez et al., 2003) suggested that the LEERT approach could successfully recover anomalies when the inter-electrode distance is about 145 m and the reservoir depth was 1350 m. The Phase 1B scenarios considered here have inter-electrode distance of about 680 m, about 4.7 times larger while the reservoir depths are similar (1420 m versus 1350 m). The much longer distances greatly reduce the current density in the inter-electrode regions thereby reducing sensitivity.

The right image in Figure 9 shows the current density predicted for the deployment 3 scenario: short electrodes are lowered below the bottom of the abandoned well casings. These electrodes are connected to the surface by insulated cable. The image shows that the current density in the immediate vicinity of the point electrodes location has increased. However, the current density of the regions between electrodes has decreased. This means that the combined point/long electrodes assumed by deployment 3 offer better sensitivity very close to the point electrodes and poorer sensitivity between electrodes.

The current density images also help to illustrate the influence that other metallic casings such as those in oil producing wells can have on current flow. Such casings may act as high conductivity pathways that will distort the current field near the wells. Figure 10, left image, repeats the current density map corresponding to deployment 1 scenario, where the top of the reservoir and the bottom of the casings are located at 1420 m. We then recalculated density assuming that the casings in the producers were magically removed from the field and calculated the differences between these two cases. These differences are shown by the right side image in Figure 10. Note that the producer casings increase the current density locally, thereby distorting the current flow that would otherwise develop. These distortions produce high voltage/current gradients that are difficult to simulate numerically and affect the capacity to resolve CO_2 plumes.

In summary, the current density maps suggest that:
a) Low current densities in the reservoir layer tend to produce measurements with low SNR. b) Highest sensitivity predicted close to the electrodes, less sensitivity to the inter-electrode regions. c) Sensitivity is inversely proportional to casing length, shorter casings and shallower reservoir layer provide better chances of detecting the CO2 plume. d) The presence of other metallic casings (not used as electrodes) distort the current field can affect the capacity to resolve the shape of the plumes. e) Deployments 1 and 2 produce very similar current density, deployment 3 produces the lowest current density. f) Possible modifications to the abandoned wells were evaluated; these are not likely to improve sensitivity to the CO_2 in the reservoir layer.

Tomograms – electrical resistivity change

The results so far suggest that it will be difficult to detect and resolve the CO_2 plumes in the Phase 1B area. For the sake of completeness, we nevertheless examine

the performance of the LEERT inversions. We first calculated synthetic data assuming the resistivity model shown in Figure 5, with and without the pink areas corresponding to the CO_2 plume. This was done for all deployment scenarios, even though we already determined that there is insufficient information for successful inversion.

We then use these data to compute tomograms of electrical resistivity change using the approach described by Ramirez et al. (2003). The inversions produce 2D tomograms; the calculations are done using 3D techniques but the long electrodes produce data that do not offer any vertical resolution.

Figures 11 – 14 show the images produced. As expected, the results show weak, distorted resistivity anomalies that bear little resemblance to the real anomalies (shown in outline form by the white rectangles). This is mostly due to a lack of information caused by the challenging conditions present at the Phase 1B area: long casings, deep reservoir layer, the large inter-electrode distance and the presence of other casings that distort the field. We note that simulations shown by Ramirez et al. suggest that the LEERT method can produce useful plume images when shorter casing lengths and shorter inter-electrode distances are considered.

Alternative approaches

We believe that the primary driver limiting the usefulness of LEERT in the Phase 1B area is the large inter-electrode distances. The obvious way to reduce these distances is to include additional casings as long electrodes. The oil producer casings shown in Figure 2 could be used as additional electrodes thereby reducing the inter-electrode distance in areas where producers exist. Our past experiences indicate that field operators are unlikely to allow us to access these wells as electrodes due to operational and safety concerns. Thus, these casings were not included in the deployment scenarios considered.

We now consider recent developments that may improve the chances of obtaining useful Phase 1B plume images. The criteria used to ascertain the quality of the data in section “Predicted signal-to-noise and current density”, are probably too conservative given recent advances in ERT data acquisition technology. The criteria used are based on field experiments conducted about 8-10 years ago where it was necessary to send field crews onsite to collect the data. Practically, this limited the amount of signal stacking (time-averaging) to several hours. New instrumentation offers the capability of remote and autonomous data collection once the instrumentation has been installed on-site. This means that, for slow moving plumes such as those at Weyburn, it is possible to do signal stacking over periods of days to weeks. This will likely improve the SNR of the measurements thereby increasing the tomograms’ resolution and sensitivity.

Joint inversion of LEERT data and other independent data may produce better images if the additional data provides new information about the target of interest.

For example, Ramirez et al., 2007 showed that CO_2 plume that could not be imaged successfully using LEERT data and a stochastic inversion approach. However, when the LEERT data was jointly inverted with injected CO_2 volume information, useful images of the plume could be produced. This approach was not tried here because it is outside of the scope of the work. The stochastic inversion approach can also use other types of data such as geophysical logs, cross-well seismic data, surface or down-hole tilt data, and InSAR data. Joint inversions of LEERT and one or more of these data sets is more likely to produce useful images than LEERT data inverted by itself.

Summary

We have conducted a numerical modeling study that evaluated whether LEERT could be used successfully to monitor CO_2 distribution in the Weyburn-Midale reservoir, Phase 1B area and assessed the sensitivity and resolution of the method.

Using Phase 1B - specific information we developed a set of models representing realistic CO_2 injection scenarios. We consider two distinct well configurations: 1) Eight abandoned wells near the Phase 1B area were used to "collect the data". 2) An additional 22 WAG wells were also used to conduct the surveys; this scenario is called deployment 1. We also consider a case were the casing length and reservoir depth is only 820 m (shallowest depth at which CO_2 will remain supercritical) to assess the effect of the length of the casings on the results. This scenario is called deployment 1-shallow). 3) Another scenario assumes that a steel wire rope reaches below the end of abandoned casing into the reservoir layer; this scenario is called "deployment 2". 4) The last scenario assumes short electrodes lowered to reservoir depths and connected to the surface via insulated cables; this scenario is called deployment 3. For each scenario, the modeling predicted the electrical response at two times: (a) after 1.4 years of CO_2 injection, and (b) after 5.7 years of CO_2 injection. We assume that the super-critical CO_2 increases the resistivity by a factor of about 4, based on the work of Albright (1986).

The following conclusions are based on the modeling study. The results suggest that none of the deployment scenarios considered are likely to produce enough data with adequate SNR and sensitivity to allow successful inversion of ERT data. A small fraction of the measurements produced by deployments 1 and 2 will be able to detect the CO_2 anomalies while deployment 3 does not offer any detection capability. It appears that the number of "good" measurements is insufficient to resolve the shape and location of the plume.

As expected, inversion of the synthetic data produces plume images that are smaller in magnitude than the "true" model and are highly distorted. This is mostly due to a lack of information caused by the challenging conditions present at the Phase 1B area: long casings, deep reservoir layer, the large inter-electrode distance, the reservoir layer being more resistive than the overburden, and the presence of other casings that distort the field.

The large inter-electrode distance is likely to be the dominant condition responsible for low measurement sensitivity. Previous work (Ramirez et al., 2003) suggested that the LEERT approach could successfully recover anomalies when the inter-electrode distance is about 145 m and the reservoir depth was 1350 m. The Phase 1B scenarios considered here have inter-electrode distance of about 680 m, about 4.7 times larger while the reservoir depths are similar (1420 m vs 1350 m). The much longer distances greatly reduce the current density in the inter-electrode regions thereby reducing sensitivity.

The modeling also illustrates that: a) Low current densities in the reservoir layer produce measurements with low SNR. b) Highest sensitivity predicted close to the electrodes, less sensitivity to the inter-electrode regions. c) Sensitivity is inversely proportional to casing length, shorter casings and shallower reservoir layer provide better chances of detecting the CO2 plume. d) The presence of other metallic casings (i.e., producer well casings not used as electrodes) distort the current field can affect the capacity to resolve the shape of the plumes.

Acknowledgements

We are grateful for the funding support provided by the Petroleum Technology Research Center, Saskatchewan, Canada. We are also grateful for the data provided by Barbara Dietiker and for the guidance provided by Dr. Don White, both at the Geological Survey of Canada. This work has been performed under the auspices of the U.S. Department of Energy by Lawrence Livermore National Laboratory under Contract DE-AC52-07NA27344.

Disclaimer

References:

Albright, J. C., 1986, Use of well logs to characterize fluid flow in the Maljamar CO_2 Pilot, *J. Pet. Tech*., vol. 38, no. 9, p. 883, 890.

Binley, A., S. Henry-Poulter and B. Shaw, 1996, Examination of solute transport in an undisturbed soil column using electrical resistance tomography, *Water Resour. Res.*, **32**(4), 763-769.

Binley, A., P. Winship, M. Pokar and J. West, 2001b, Cross-borehole radar and resistivity tomography: A comparison of techniques in unsaturated sandstone, In: Proc. Symp. Applications of Geophysics to Engineering and Environmental Problems (SAGEEP2001), Environmental and Engineering Geophysical Society, Denver, CO.

Daily, W. A. Ramirez, D. LaBrecque and J. Nitao, 1992, Electrical resistivity tomography of vadose water movement, *Water Resour. Res.*, **28**(5), 1429-1442.

Daily, W., A. Ramirez, R. Newmark and V. George, 2000, imaging UXO using electrical impedance tomography, *J. Environmental and Engineering Geophysics,* **5**(4)*,* 11-23.

Kemna, A, A.Binley, A.Ramirez and W.Daily, 2000, Complex resistivity tomography for environmental applications, *Chemical Engineering Journal*, **77**(1-2), p11-18.

LaBrecque, D. J., Miletto, M., Daily, W. D., Ramirez, A. L., and Owen, E., 1996, The effects of noise on Occam's inversion of resistivity tomography data, *Geophysics*, **61**, 538-548.

LaBrecque, D., G. Morelli, W. Daily, A. Ramirez, and P. Lundegard, 1999, Occam's inversion of 3D Electrical Resistivity Tomography, in "Three-dimensional electromagnetics", eds. M. Oristaglio, B. Spies, and M.R. Cooper, Soc. Of Exploration Geophysicists, pages 575-590.

LaBrecque, D.J. and Yang, X, 2000, Difference inversion of ERT data: A fast inversion method for 3-D in-situ monitoring, In: *Proceedings of the Symposium on the Application of Geophysics to Engineering and Environmental Problems*, Env. Eng. Geophys. Soc., 907-914.

Loke, M.H. and R.D. Barker, 1995, Rapid least-squares inversion of apparent resistivity pseudosections by a quasi-Newton method, *Geophys. Prosp.*, **44**, 131-152.

Oldenburg, D.W. and Y. Li, 1994, Inversion of induced polarization data, *Geophysics*, **59**, 1327-1341.

Ramirez, A., W. Daily, D. LaBrecque, E. Owen and D. Chesnut, 1993, Monitoring and underground steam injection process using electrical resistance tomography, *Water Resources Research,* **29(1)**, 73-87.

Ramirez, A., W. Daily, D and R. Newmark, 1995, Electrical resistance tomography for steam injection monitoring and process control, *J. Environ. Eng. Geophys.,* **0**, 39-51.

Ramirez, A., W. Daily, A. Binley, D. LaBrecque and D. Roelant, 1996, Detection of Leaks in Underground Storage Tanks Using Electrical Resistance Methods, *J. Engineering and Environmental Geophysics, **1,*** 189-203.

Ramirez, A., and W. Daily, 2001, Electrical Imaging of the Large Block Test-Yucca Mountain, Nevada, *Journal of Applied. Geophysics ,* **46***,* 85-100.

Ramirez, A., R. Newmark, and W. Daily, 2003, Monitoring carbon dioxide floods using electrical resistance tomogramy (ERT): Sensitivity studies, *Journal of Enviromental. and Eng. Geophysics* ,vol. 8, no. 3, pp. 187 - 208.

Ramirez, A., W. Foxall, K. Dyer, and S. J. Friedmann, Monitoring and reconstruction of subsurface CO2 plumes using a stochastic inversion approach, Proc. 2007 AAPG Annual Convention, Long Beach, CA, April 1 – 4, 2007.

Sasaki, Y., 1994, 3-D resistivity inversion using the finite-element method, *Geophysics*, **59**(11), 1839-1848.

Schima, S., LaBrecque, D. J, and Lundegard, P. D., 1996, Using resistivity tomography to monitor air sparging, *Ground Water Monitoring and Remediation*, **16**, 131-138.

Shi, W., W. Rodi, M. Toksoz, and D. Morgan, 1997. Three dimensional electrical resistivity tomography and its application to Larderello-Valle Secolo geothermal field in Tuscany, Italy, Symposium on the Application of Geophysics to Engineering and Environmental Problems (SAGEEP) '97, Reno, NV., March 23 – 26, 1997, Vol. II, 889-899.

Slater, L., Zaidman, M.D., Binley, A.M. and West, L.J., 1997a, Electrical imaging of saline tracer migration for the investigation of unsaturated zone transport mechanisms, *Hydrology and Earth System Sciences*, **1**, 291-302.

Slater, L., A. Binley, D. Brown, 1997b, Electrical Imaging of the Response of Fractures to Ground Water Salinity Change, *Ground Water*, **35**(3), 436-442.

Tikhonov, A. N. and Arsenin, V. Y., 1977, *Solutions of ill-posed problems*, ed. Fritz, J., John Wiley & Sons, New York.

Figures

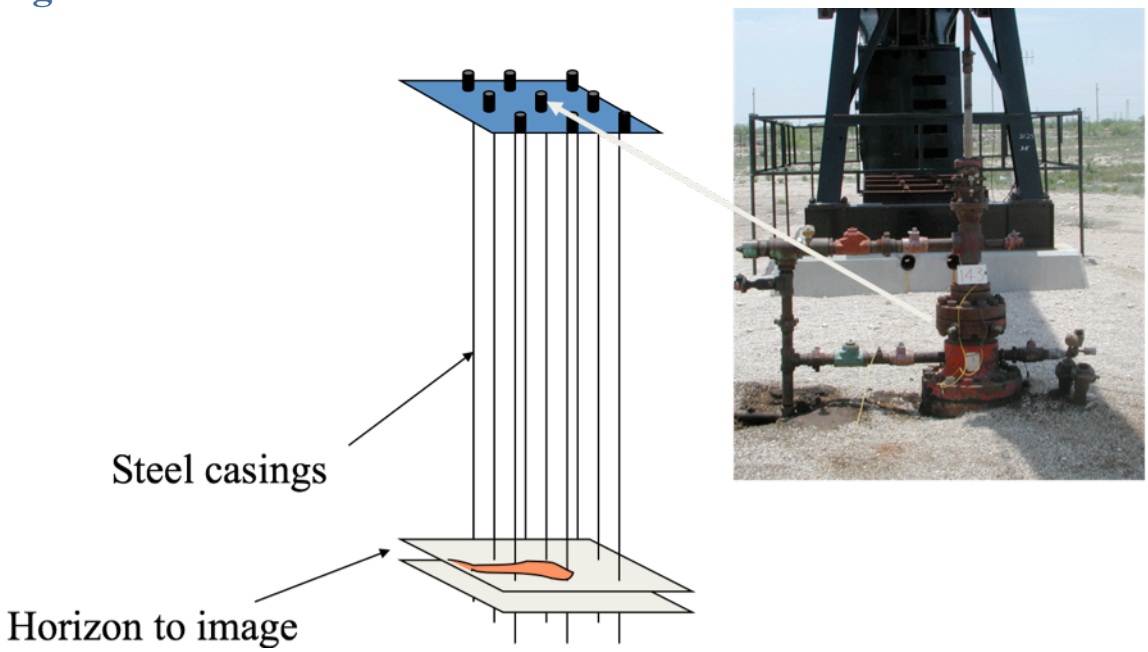

Figure 1. Schematic view of the LEERT approach. Steel-cased wells are used as long electrodes to survey the electrical resistivity of rock between the casings. The method offers some lateral resolution but does not does not provide vertical resolution.

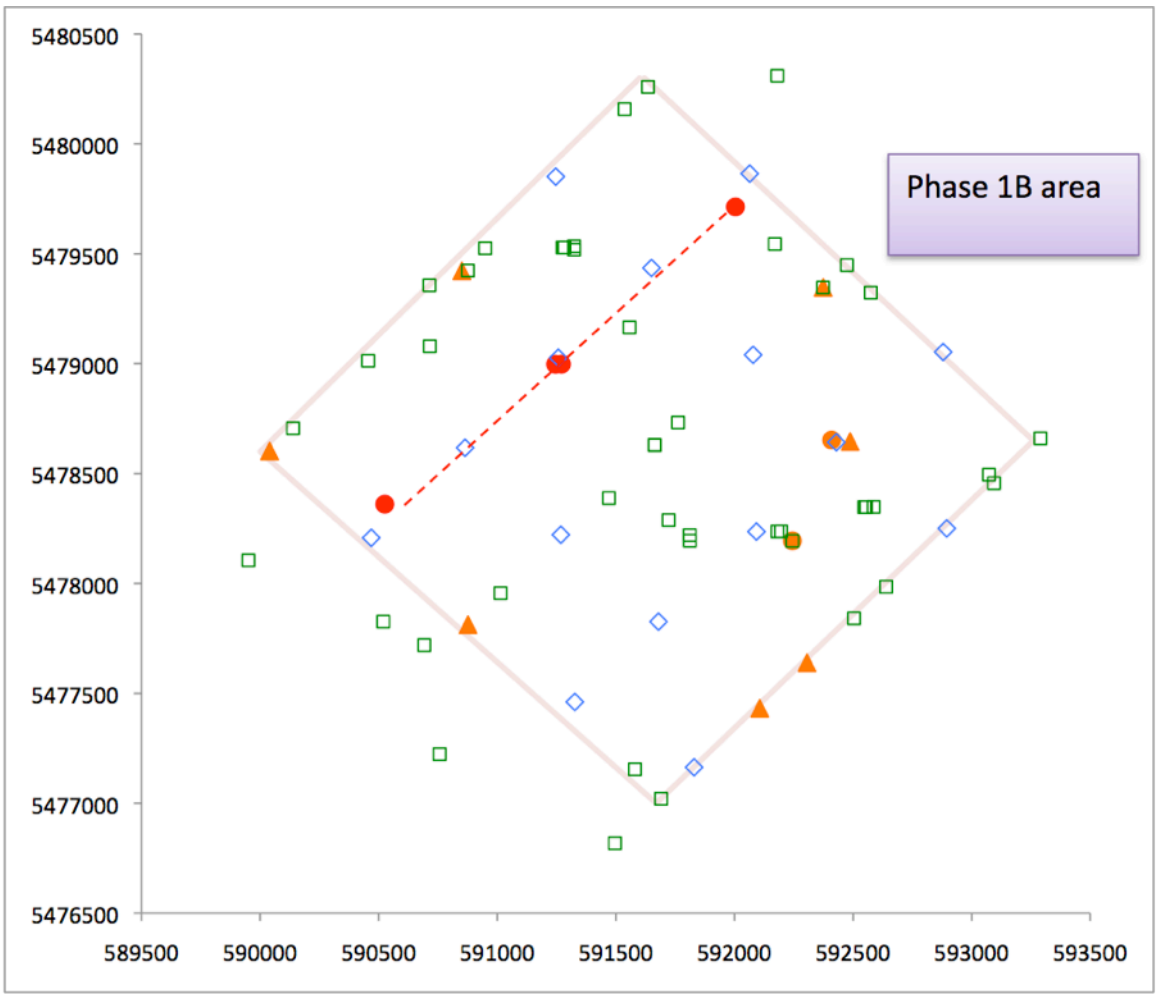

Figure 2. Map view of the Phase 1B area showing the location of wells containing metallic casing: abandoned wells (orange triangles), water injection wells (blue diamonds), observation wells (orange circles) and oil producers (green squares). CO_2 injection wells active during the time-period of interest are shown in red; the dashed red line indicates that the horizontal part segment of the injectors is uncased.

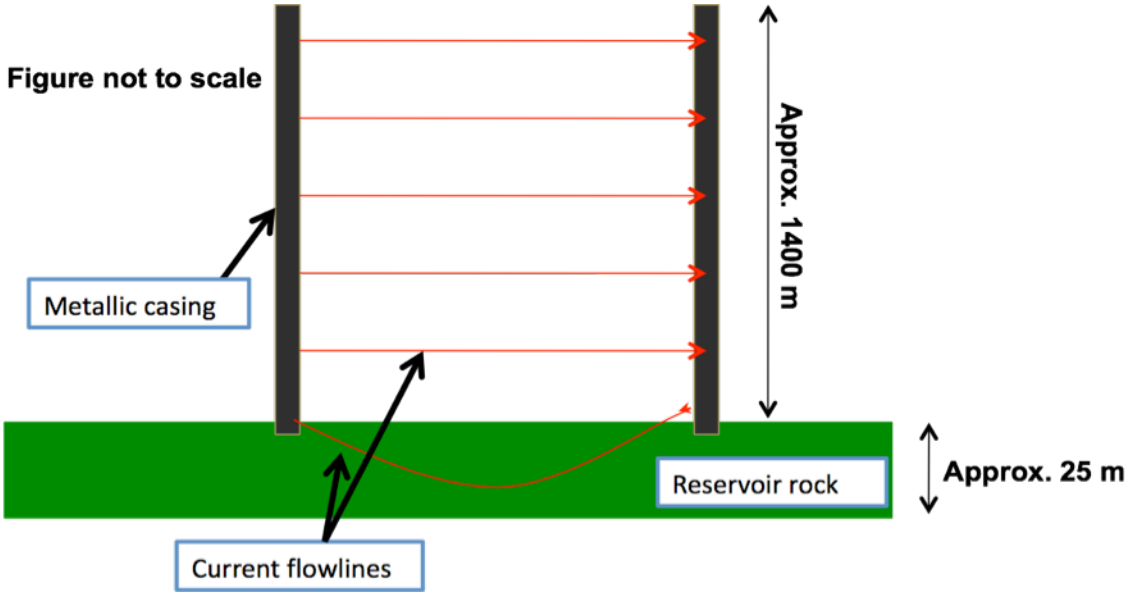

Figure 3. Schematic view of current flow. Almost all of the current flows through the overburden rock. A small amount of current samples the reservoir.

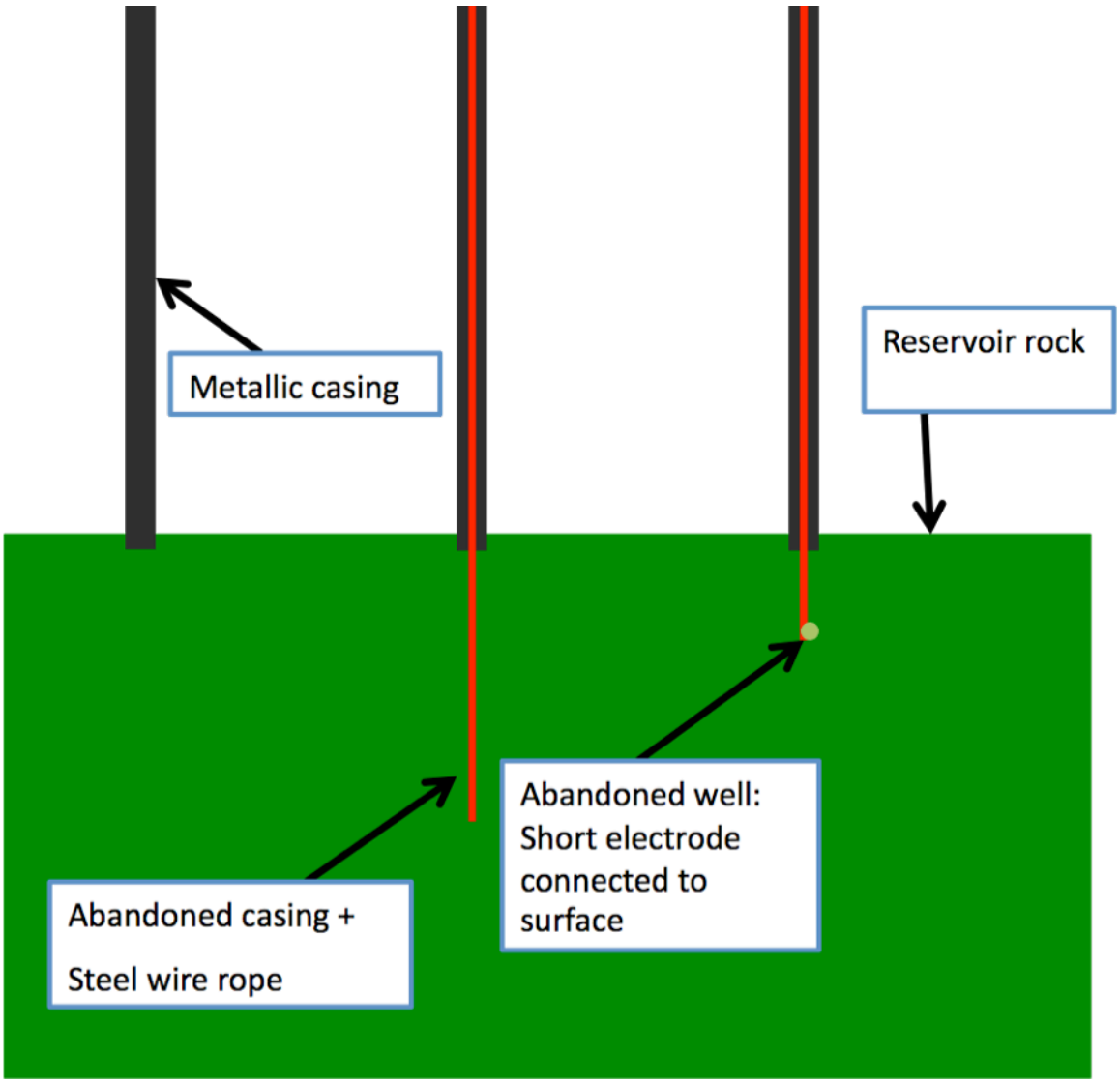

Figure 4. We consider three electrode scenarios. One scenario assumes that the electrodes consist of metallic casing that terminates near the top of the reservoir (left part of the figure); this scenario is called Deployment 1. A second scenario assumes that a steel wire rope reaches into the reservoir thereby increasing reservoir current flow (center part of the figure); this scenario is called Deployment 2. A third scenario assumes that a short electrode is lowered to the uncased section of the well; the electrode is connected to the surface by an insulated cable; this scenario is called Deployment 3.

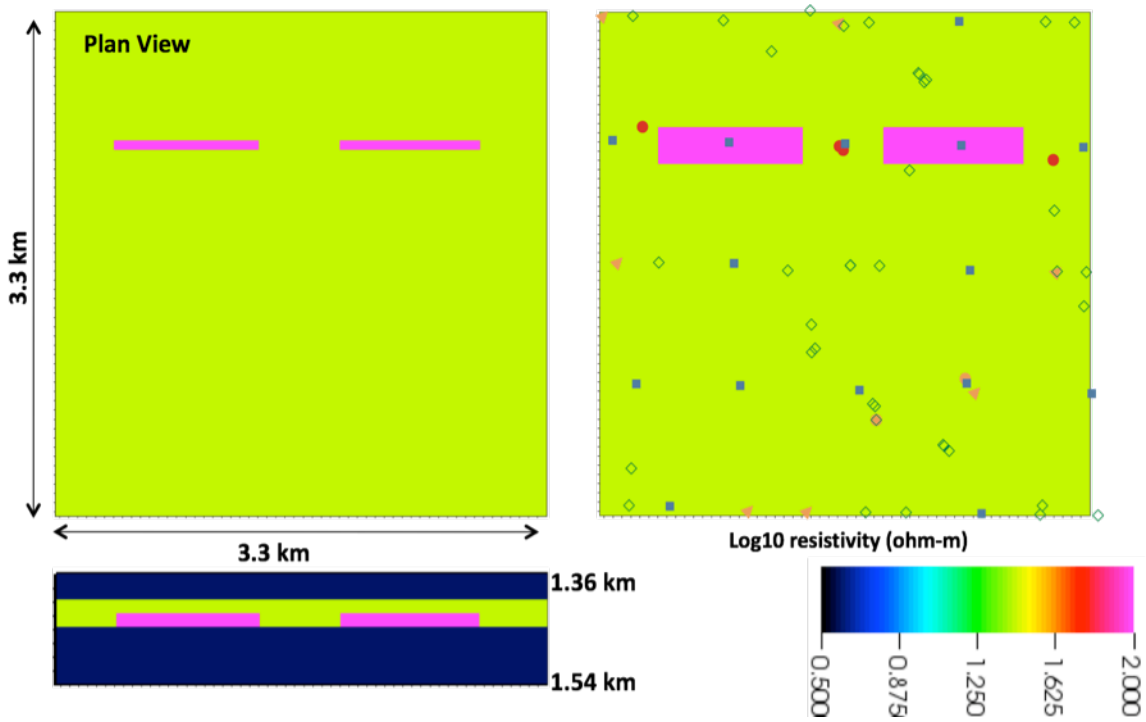

Figure 5. We consider two injection scenarios. The top left frame shows a horizontal slice intersecting the reservoir layer and resistivity anomaly caused by the CO_2 injection over a 1.4 year period. We assume that the CO_2 causes a fourfold increase in resistivity. The bottom left figure shows a vertical slice across the anomaly locations. The top right frame shows a resistivity anomaly caused by the CO_2 injection over a 5.7 year period. The metallic casings are shown on the right: abandoned wells (yellow triangles), WAG wells (blue squares), producers (green open diamonds), cased-section in CO_2 injectors (red circles).

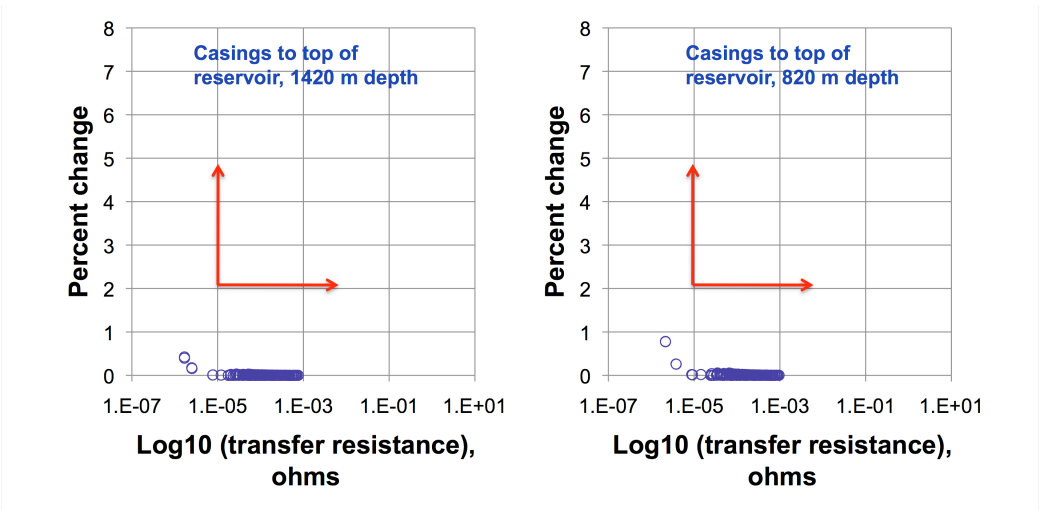

Figure 6 compares the magnitude of the predicted resistances and the predicted change in resistivity caused by 5.7 years of CO_2 injection. Only the 8 abandoned well casings were used as electrodes. The results on the left represent "Deployment 1" and those on the right "Deployment 1-shallow". Any resistance measurements with magnitudes > 10^{-5} and percent changes larger than 2% (points above and to the right of the red arrows) are likely to have acceptable signal to noise ratios (SNR). The plots suggest that none of the measurements are likely to have acceptable SNR.

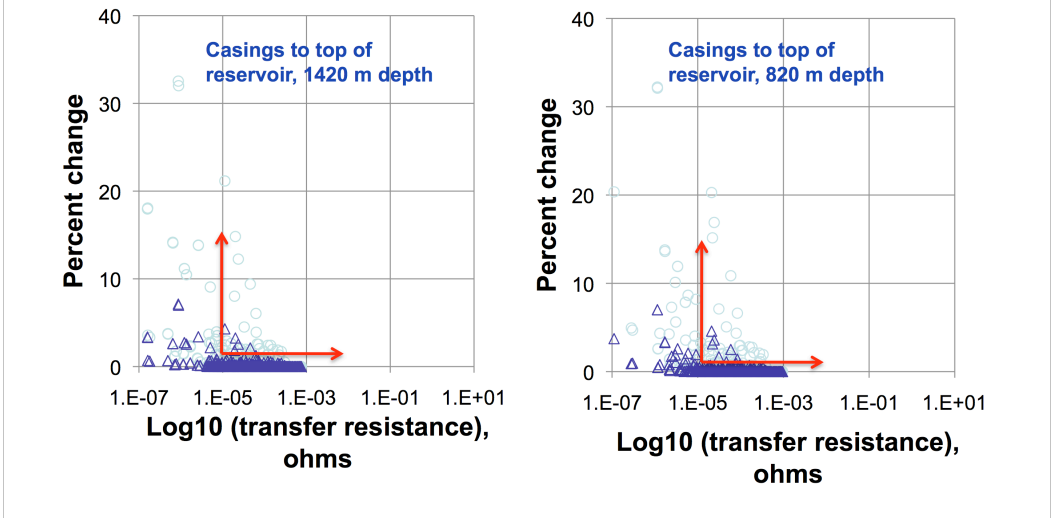

Figure 7 compares the magnitude of the predicted resistances and the predicted change in resistivity caused by 1.4 and 5.7 years of CO_2 injection (dark blue triangles and light blue circles, respectively). Eight abandoned well casings and 14 WAG well casings were used as electrodes. The results on the left represent "Deployment 1" and those on the right "Deployment 1-shallow". Any resistance measurements with magnitudes > 10^{-5} and percent changes larger than 2% (points above and to the right of the red arrows) are likely to have acceptable signal to noise ratios (SNR).

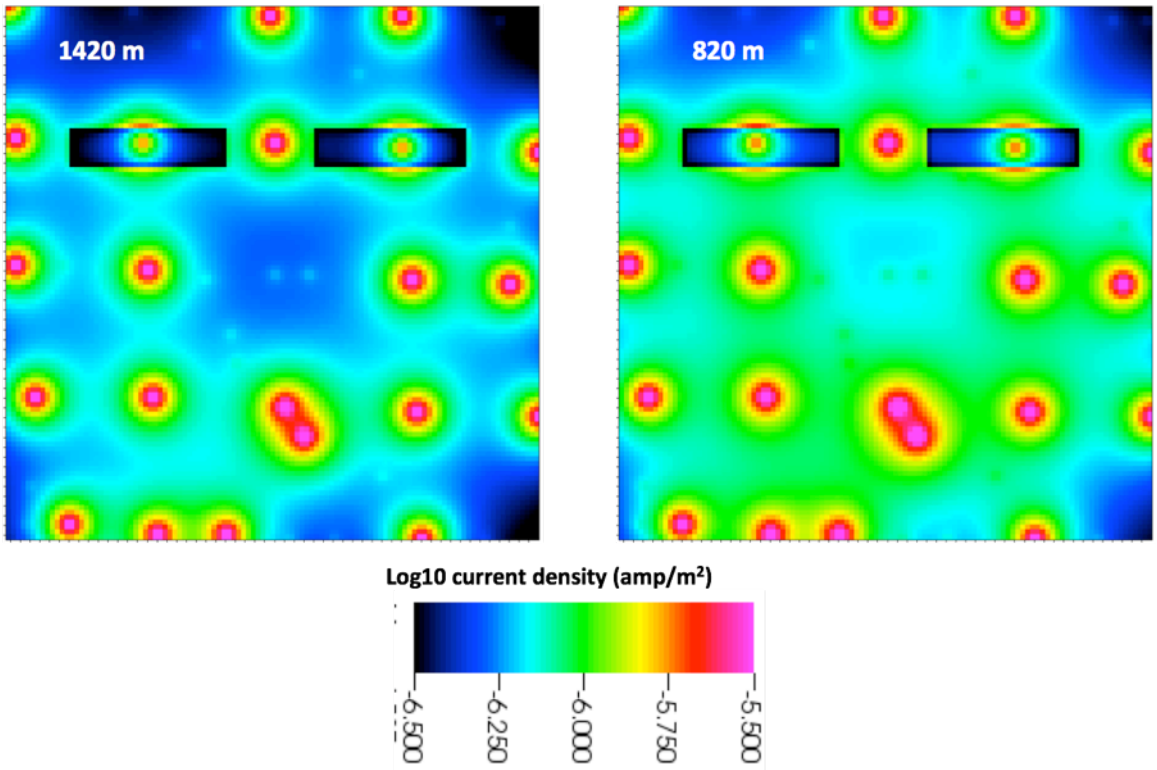

Figure 8. The two horizontal slices show current density in the reservoir. We assume that the abandoned wells and water injection wells are used as long electrodes. The scenario on the left assumes that the top of the reservoir and the bottom of the casings are located at 1420 m (deployment 1 scenario). The scenario on the right assumes that the top of the reservoir and the bottom of the casings are located at 820 m (deployment 1-shallow scenario). Larger current densities exist when the reservoir is shallower.

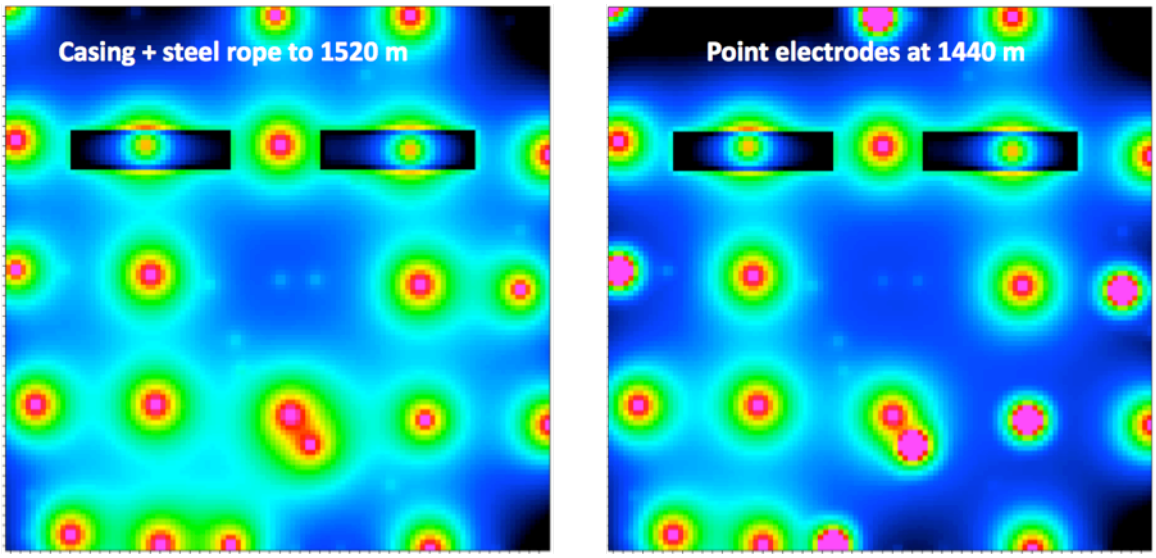

Figure 9. The two horizontal slices show current density in the reservoir. We assume that the abandoned and WAG wells are used as long electrodes. The scenario on the left

assumes deployment 2 scenario: the top of the reservoir and the bottom of the casings are located at 1420 m, and that a steel wire rope has been inserted into each abandoned well to improve the electrical coupling with the reservoir layer. The image on the right shows the density for deployment 3 scenario: short electrodes are lowered below the bottom of the abandoned well casings; these electrodes are connected to the surface by insulated cable. The location of the abandoned wells is indicated by the yellow triangles in Figure 5.

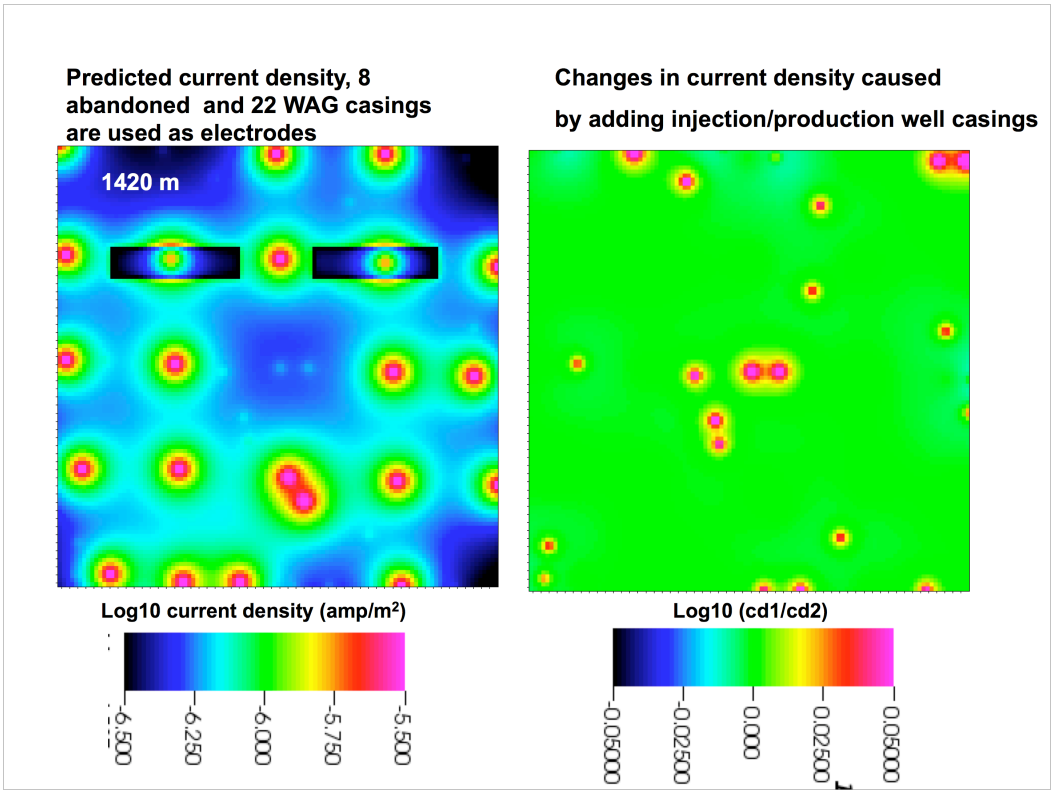

Figure 10. The image on the left shows the current density associated with the deployment 1 scenario. The image on the right shows the changes in current density caused by adding the metallic casings in the oil producer wells. These wells act as high conductivity pathways that locally distort the current field within the reservoir.

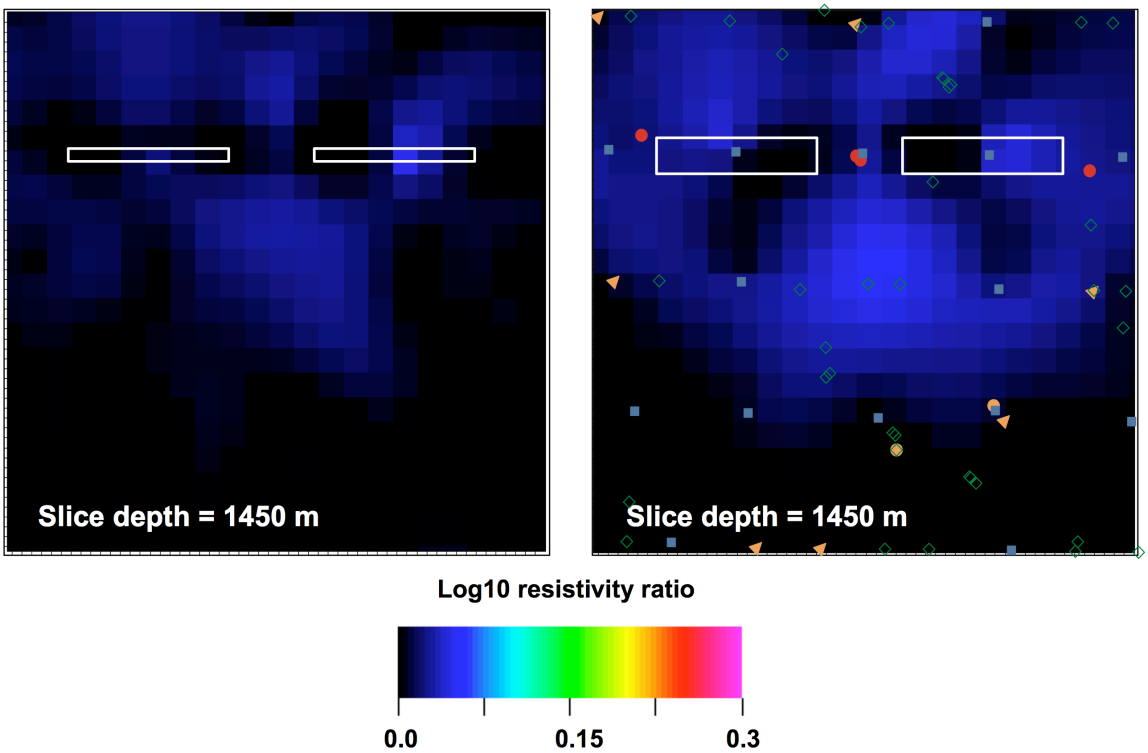

Figure 11. The images show the changes recovered using deployment 1 data; 22 casings (8 abandoned (orange triangles), 22 WAG (blue squares)) end at the top of the reservoir (1420 m). The left and right images show resistivity changes due to 1.4 and 5.7 years of injection, respectively. The true resistivity ratio is log10(4) = 0.6.

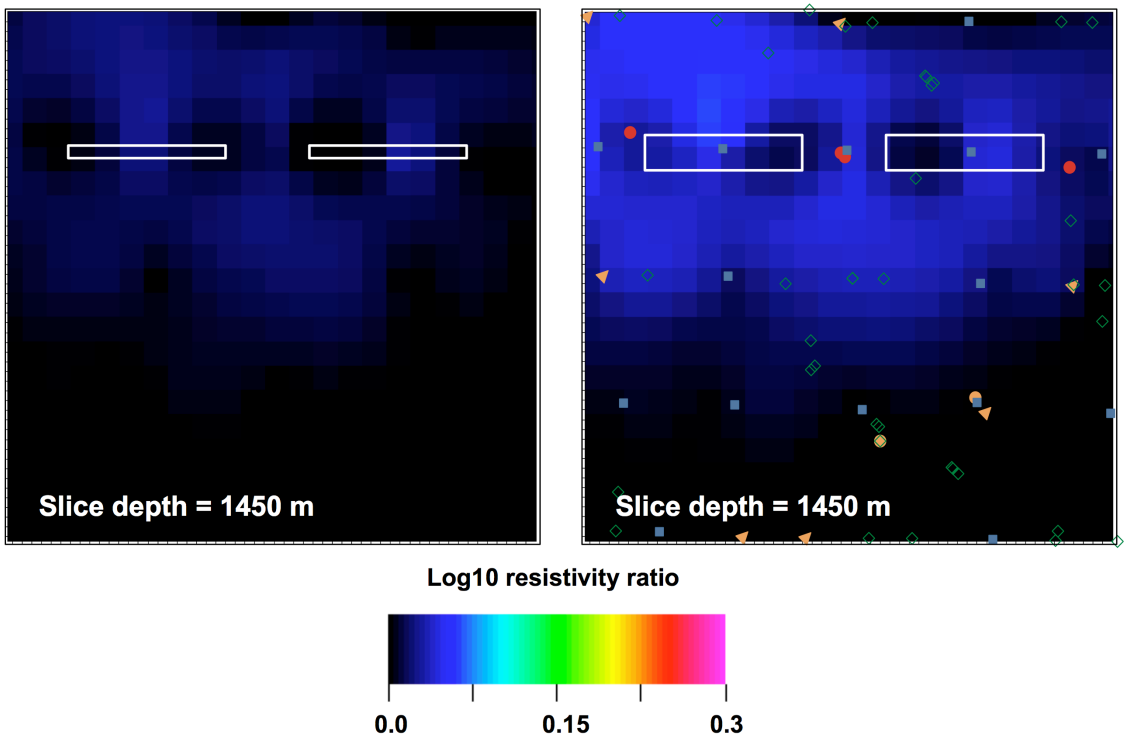

Figure 12. The images show the changes recovered using deployment 2 data: steel wire rope has been added to 8 abandoned wells (orange triangles) to increase the electrical coupling with the reservoir. The left and right images show resistivity changes due to 1.4 and 5.7 years of injection, respectively. The true resistivity ratio is log10(4) = 0.6.

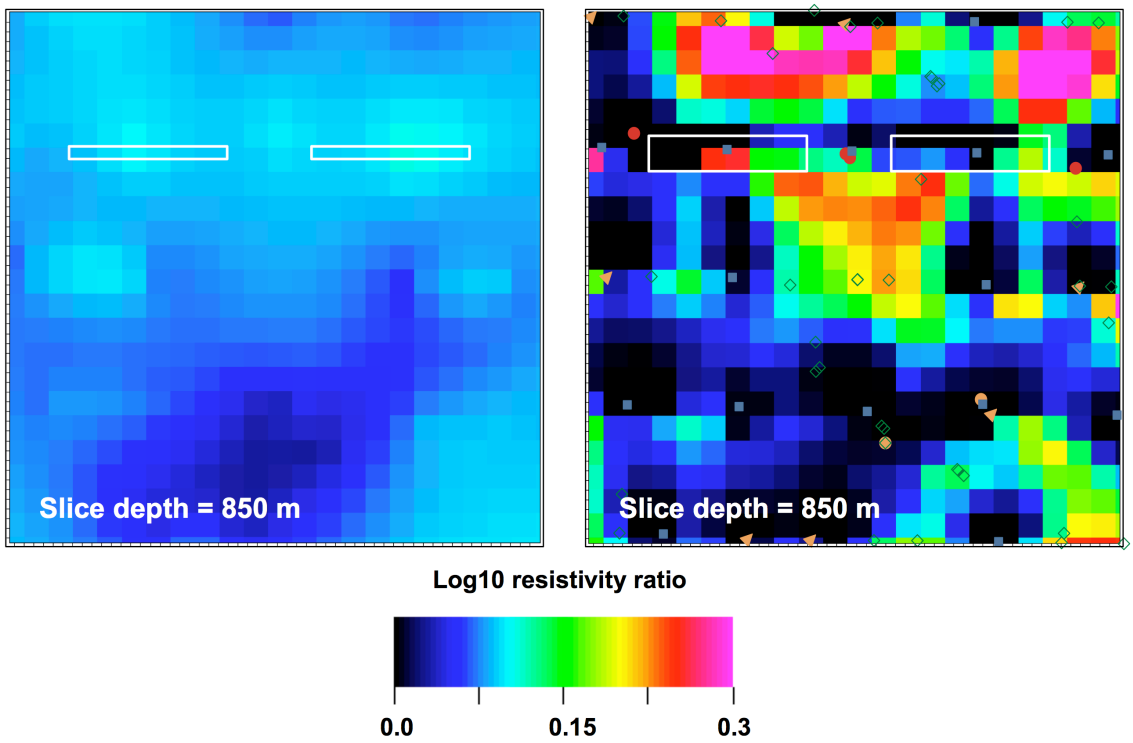

Figure 13. The images show the changes recovered using deployment 1-shallow data: the 22 casings (8 abandoned (orange triangles), 22 WAG (blue squares)) end at the top of the reservoir (820 m). The left and right images show resistivity changes due to 1.4 and 5.7 years of injection, respectively. The true resistivity ratio is log10(4) = 0.6.

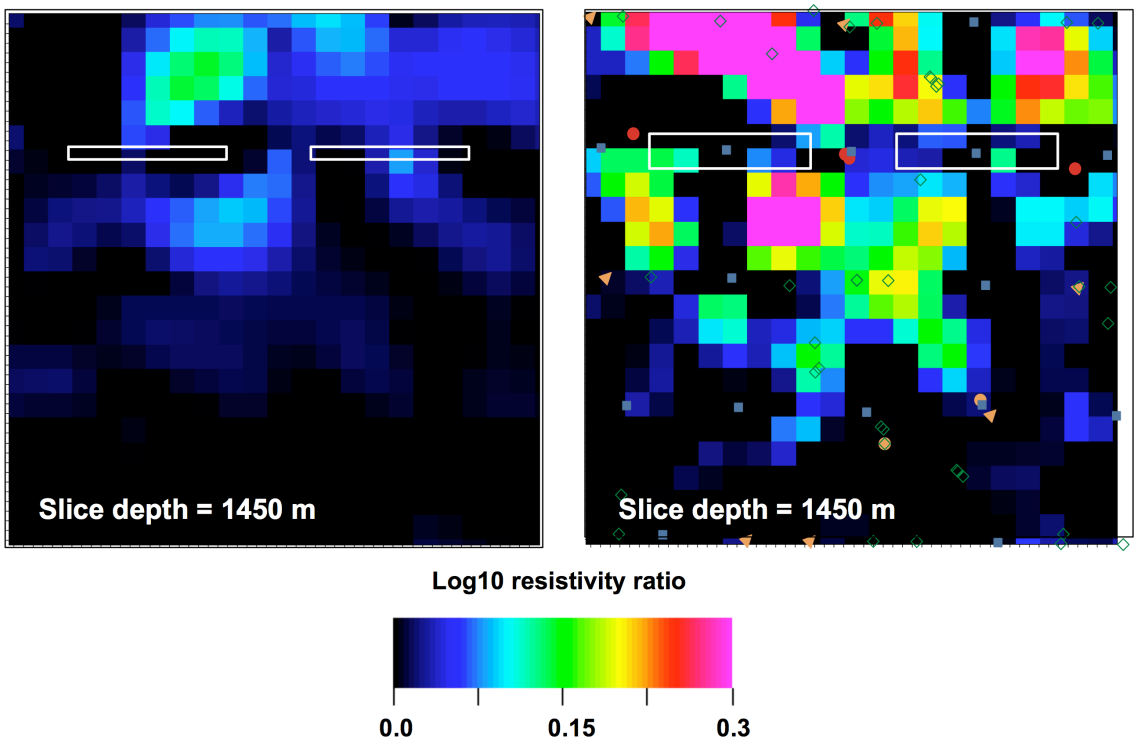

Figure 14. The images show the changes recovered using deployment 3 data: short electrodes been added to 8 abandoned wells (orange triangles) to increase the electrical coupling with the reservoir. The left and right images show resistivity changes due to 1.4 and 5.7 years of injection, respectively. The true resistivity ratio is log10(4) = 0.6.